Spatial and Temporal Coarse Graining for Dispersion in Randomly Packed Spheres

Ulrich M. Scheven and Pabitra N. Sen

Schlumberger-Doll Research, Old Quarry Road, Ridgefield, Connecticut 06877

(Received 29 May 2002; published 27 November 2002)

The propagator for molecular displacements $P(\zeta, t)$ and its first three cumulants were measured for Stokes flow in monodisperse bead packs with different sphere sizes d and molecular diffusion coefficients D_m. We systematically varied the normalized mean displacement $\langle\zeta\rangle/d$ and diffusion length $L_D = \sqrt{2D_m t}/d$. The experimental results map onto each other with this scaling. For $L_D/d < 0.2$ the propagator remains non-Gaussian, and thus an advection diffusion equation is not obeyed, for mean displacements measured up to $\langle\zeta\rangle > 10d$. A Gaussian shape is approached for large mean displacements when $L_D > 0.3d$.

DOI: 10.1103/PhysRevLett.89.254501 PACS numbers: 45.70.Cc, 05.40.–a, 47.55.Mh, 66.20.+d

Dispersion, the transport of molecules or tracers due to combined effects of diffusion and fluid flow at low Reynold's number, is an important problem both in the fundamentals of hydrodynamics [1–3] and in its application in diverse fields ranging from biological perfusion, chemical reactors to soil remediation, and oil recovery. The probability distribution of displacements in the long time and large displacement regime is expected to become a Taylorian; i.e., its dynamics are given by a coarse-grained advection diffusion equation giving rise to a Gaussian distribution whose center moves at the average velocity, and whose mean square displacement σ^2 is given by a time-independent dispersion coefficient $D = \sigma^2/2t$. de Gennes [3] pointed out that this simple picture is "upset" in a porous medium when stagnation zones are present. In many experiments [4–10] and simulations [11,12] on packed spheres—the simplest random porous medium—the distribution appears to be non-Gaussian and non-Taylorian in certain regimes, and not in others. The purpose of this Letter is to investigate how the distribution of displacements evolves under controlled and systematic variation of spatial and temporal coarse-graining parameters. We delineate different experimental regimes and assert that in most of the recent experiments the distribution remains essentially non-Taylorian.

The streamlines of Stokes flow ($R_e \ll 1$) in a porous medium provide a quenched random system [13,14] in which molecules hop between streamlines and flow channels by random walks. In this regard the slow flow problem in complex geometries is analogous to turbulent diffusion [15]. In the absence of diffusion, mechanical mixing leads to dispersion as molecules move downstream and sample various regions of the flow field. The spatial coarse-graining length is defined by the mean flow distance $\langle\zeta\rangle$ with which a representative section of the flow field is sampled. The diffusional coarse graining is measured by the diffusion length $L_D = \sqrt{2D_m t}$, where t is the time scale of the experiment. Our experiments are conducted with these coarse grainings in mind and cover a parameter space $\{\langle\zeta\rangle, L_D\}$ encompassing that of prior experimental and numerical work and providing a unifying picture of the preasymptotic dispersion processes.

The experiments were performed on two random packs prepared by pouring glass spheres of $d = 152 \pm 12$ μm or $d = 215 \pm 15$ μm into Teflon tubes of 18 mm diameter, tapping them down and sealing the ends with sieves to keep them in place. Subsequently the packs were filled with water ($D_m \simeq 2.1 \times 10^{-9}$ m^2/s) or dodecane ($D_m \simeq 0.8 \times 10^{-9}$ m^2/s) and a homogeneous fluid saturation was confirmed using 1D NMR images. The fluid was then pushed through the pack with mean flow velocities $\bar{v}$ up to 16 mm/s and Reynolds numbers $R_e < 1$. Constant flow rates were maintained with "ISCO-1000D" piston pumps. While the fluid flowed pulsed field gradient(PFG)-NMR was used to tag the positions of the fluid's polarized protons at an initial time t_0 and to then obtain the probability distribution for displacements along the direction of the mean flow at a later time $t_0 + t$. The PFG-NMR experiments measure explicitly the stagnant volumes in the pore space and their coupling to the flow. This contrasts with traditional effluent measurements [4,16,17], which deduce these properties from effluent data and heuristic capacitance models. Various PFG techniques [18–20] have been used by several experimental groups [6,8,9,21–24] to study dispersion in porous media. We used a standard alternating pulsed gradient stimulated echo [19] pulse sequence commonly used in this type of experiment, for example, as in Refs. [8,9]; NMR details for our experiment are not out of the ordinary and will be reported elsewhere. The accuracy of the pulse sequence and measurement was confirmed with bulk diffusion measurements on water and dodecane. The velocity independence of the measured relaxation time T_1 was also verified.

The data are analyzed readily as the signal is proportional [19] to the ensemble average $\langle e^{iq\zeta}\rangle$ over all polarized spins, where $q = 2\pi\gamma\delta g_z$ is the magnetization wave vector set up by the pulsed field gradients and $\zeta = z(t) - z(0)$ is the displacement of a spin along the gradient axis z during t. γ is the gyromagnetic ratio of protons, g_z is the

amplitude of the pulsed field gradient, and δ is the effective gradient duration. The signal $\langle e^{iq\zeta}\rangle = \text{const} \times \int P(\zeta', t)e^{iq\zeta'}d\zeta'$ is measured for a set of 128 equally spaced values of q between $\pm q_{\max}$.

Propagators $P(\zeta, t)$ [25] are determined by inverse Fourier transform of the data set. The typical propagators shown in Fig. 1 demonstrate the role of diffusion in sharpening the displacement distribution. They are measured using different fluids and flow times, for the same mean flow distance $\langle\zeta\rangle/d \approx 3.2$. When flowing water or dodecane for the same time the water propagators are narrower than those measured with dodecane, which is clear evidence for better diffusive coupling of the fastest and slowest parts of the flow field to the mean flow. A similar phenomenon is observed when comparing propagators for either fluid obtained with different flow times t, where propagators appear narrower when t, and hence $L_D = \sqrt{2D_m t}$, is increased. Finally, water and dodecane propagators overlap rather well when their respective diffusion lengths are nearly the same, confirming that the shape of the propagator depends on L_D. We also note that the diffusive narrowing no longer occurs once L_D has grown to be an appreciable fraction of the sphere diameter, for example, in the near identical water propagators obtained at $L_D/d = 0.57$ and $L_D/d = 0.43$. A distorted and visibly non-Gaussian shape is observed for small L_D, most obviously so in the dodecane propagator obtained for $t = 0.1s$, $L_D/d \simeq 0.08$, which displays a pronounced "bump" [23] at zero displacement, a depressed peak around the mean displacement, and a high displacement tail. The bump is due to stagnation zones which have not had the time to couple into the flow by diffusive exchange. Similarly the tail at high displacement originates from the fastest streamlines whose occupants have not yet sampled the slower parts of the flow field. The stagnation feature has a somewhat rounded appearance, because of windowing applied to the data before performing the Fourier transform, in order to suppress ringing. Nevertheless, the presence of the stagnation feature is clear and unambiguous.

Quantitative measurements of the deviation from a Gaussian shape are derived from a cumulant analysis of the data obtained for small q. The cumulant expansion reads [26,27] $\log\langle e^{iq\zeta}\rangle = \sum_{j=1}^{\infty} \frac{(iq)^j}{j!} X_j$, and the first three cumulants $X_1 = \langle\zeta\rangle$, $X_2 = \langle(\zeta - \langle\zeta\rangle)^2\rangle = \sigma^2$, $X_3 = \langle(\zeta - \langle\zeta\rangle)^3\rangle$ of $P(\zeta', t)$ are measured directly by fitting the real and imaginary parts of $\log\langle e^{iq\zeta}\rangle$ to a parabola and a linear plus a cubic term, respectively. This is illustrated in Fig. 2, which shows data and polynomial fits obtained for $\langle\zeta\rangle/d = 2.3$. The phase of the NMR signal [$\text{Im}(\log\langle e^{iq\zeta}\rangle)$] is plotted in Fig. 2(b), after the linear term proportional to the mean displacement, indicated by the dashed line, has been subtracted from the phase for clarity. The quantitative discussion below is based on data and fits similar to those shown in Fig. 2.

In Fig. 3 we plot the propagators' normalized second cumulant for different flow times t as a function of $\langle\zeta\rangle/d$. The experiment with dodecane in 215 μm spheres probes the preasymptotic regime with diffusion lengths L_D ranging from 7% to 26% of a sphere diameter. For $\langle\zeta\rangle/d \simeq 0.14$ and the longest diffusion length $L_D/d = 0.26$ the value of σ^2 is dominated by longitudinal diffusion and thus $\sigma^2 \simeq L_D^2$. By contrast, for $\langle\zeta\rangle/d \simeq 0.14$ and the shortest diffusion length $L_D/d = 0.07$ the width of the displacement distribution is dominated by coherent flow [6] and $\sigma^2 \gg L_D^2$. Here the displacements of protons occupying different streamlines have not been averaged much in space or time, so σ^2 reflects the instantaneous velocity distribution in the sphere pack. It varies at the pore scale due to variations in the radius of any flow channel. Neither spatial nor temporal coarse graining has taken place yet. Increasing the mean displacement enhances spatial

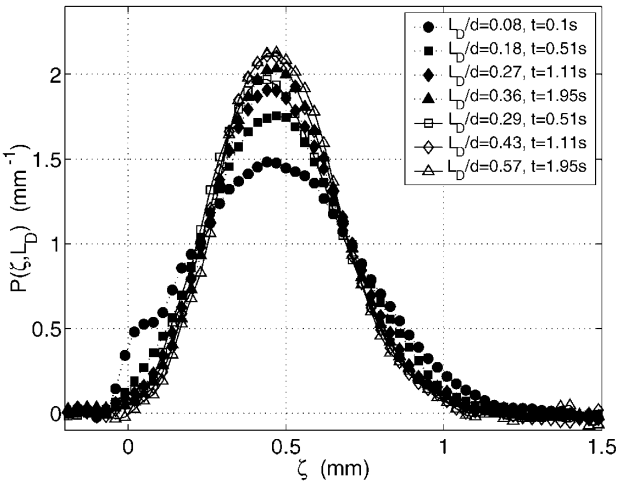

FIG. 1. Propagators at a fixed mean displacement $\langle\zeta\rangle = 490$ μm, for various diffusion times in dodecane (solid symbols) and water (open symbols). Sphere diameter $d = 152$ μm.

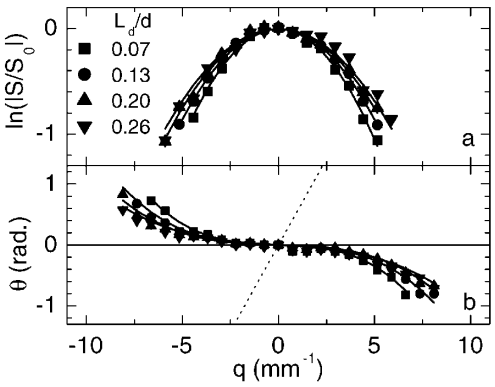

FIG. 2. NMR data and fits vs q obtained for four different diffusion lengths, at $\langle\zeta\rangle/d \simeq 2.3$. (a) NMR magnitude data shown with symbols; parabolic fits shown as solid lines. (b) NMR phase data shown with symbols, after subtraction of the linear term $\theta_{\text{lin}} = q\langle\zeta\rangle$ (dashed line). Linear + cubic fits shown as solid lines.

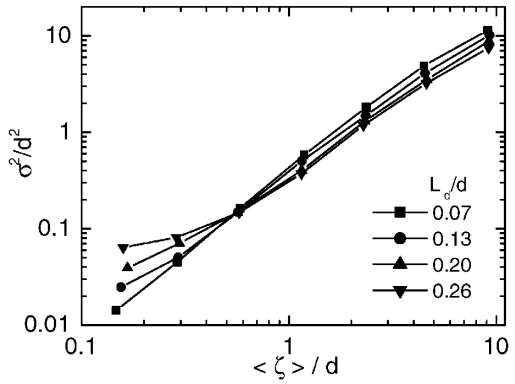

FIG. 3. Second cumulant of the displacement distribution as a function of mean flow distance and flow time.

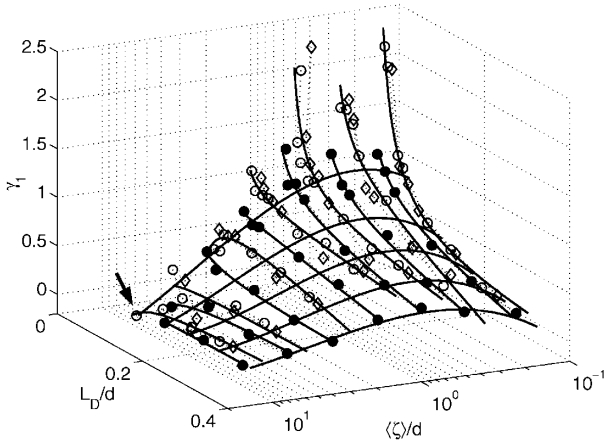

FIG. 4. Skewness $\gamma_1 = X_3/\sigma^3$ vs normalized mean displacements and diffusion lengths: ($\circ$) dodecane and $d = 215$ μm, ($\diamond$) water and $d = 215$ μm, ($\bullet$) dodecane and $d = 155$ μm. The arrow marks $\gamma_1 < 0$.

averaging, and the four curves come together and intersect at $\langle\zeta\rangle/d \simeq 0.55$. For even larger mean displacements they spread out again, but now σ^2 is smaller for larger L_D. This reflects the diffusional narrowing already illustrated in Fig. 1. Two observations can be made here. First, the diffusional narrowing can occur only when the stagnant or very slow flow zones of the velocity field are small (i.e., not macroscopic) and are located within a diffusion length of the fast-flowing backbone. For example, these zones may be located near where spheres touch [28,29]. Second, the spread of σ^2 with t at a given large distance $\langle\zeta\rangle$ is reminiscent, though it is weaker, of Saffman's logarithmic diffusive corrections [13,14,30] to dispersion, where $\sigma^2 \propto f(\langle\zeta\rangle)\log P_e$, and $P_e = \bar{v}d/D_m$ is the Péclet number.

In Fig. 4 we follow Crámer [27] and Saffman [14] and quantify the deviation from a Gaussian distribution in terms of the skewness $\gamma_1 = X_3/\sigma^3$, for three experiments, where X_3 is the third cumulant determined from the fitted cubic term of the NMR phase. The skewness is plotted against the diffusion length L_D and the mean displacement $\langle\zeta\rangle$, both normalized by the sphere diameter. All data for different sphere diameters and diffusion coefficients collapse onto a surface in the parameter space $\{\langle\zeta\rangle/d, L_D/d\}$. The solid lines are obtained by fitting suitable polynomials and power laws and serve as a guide to the eye. For small diffusion and displacement the skewness is largest. It arises from stagnation zones and from the distribution of velocities. For short diffusion lengths the skewness decreases rapidly as L_D/d is increased. This diffusion dependence is less dramatic for $L_D/d > 0.2$, but nevertheless the skewness continues to decrease as diffusion increases. As $\langle\zeta\rangle$ grows towards d the skewness first increases for all diffusion lengths, then decreases again for $\langle\zeta\rangle/d > 1$. For the largest mean displacements and $L_D/d \simeq 0.08$ the skewness becomes negative due to the continuing presence of the stagnant fluid, while steadily approaching zero for the larger diffusion lengths. This long diffusion and large displacement trend is consistent with an approach to the Gaussian shape expected for the limiting case of large displacements and long diffusion times. This is in contrast to the case of short L_D where the propagator evolves from one non-Gaussian shape with positive skewness to another non-Gaussian shape with negative skewness. The negative skewness reflects the fact that for large $\langle\zeta\rangle$ and small L_D the fluid "left behind" in stagnation zones has considerable weight in the third cumulant. Here the propagator will look approximately bimodal, with a displaced Gaussian centered far from the origin and a peak at the origin whose area is proportional to the stagnant volume, and whose width is proportional to its size.

Figure 4 provides a convenient phase diagram in which to unify and understand various dispersion experiments and simulations performed on randomly packed monodisperse spheres. PFG-NMR experiments performed to date are consistent with our results but have traversed the parameter space $\{L_D, \langle\zeta\rangle\}$ on parabolic trajectories (constant velocity, variable t) or straight line trajectories (constant t, variable velocity) and have, with the exception of the work by Ding and Candela [21], explored dispersion in the limit of short diffusion lengths where the propagators are not Gaussian and where consequently all measurements of $\sigma^2(t)$ will depend on the details of the experimental path taken through parameter space $\{L_D, \langle\zeta\rangle\}$.

Measurements of $\sigma^2(t)$ have been sought in order to find the dispersion $D \propto \sigma^2(t)/t$, because the dependence of $D(P_e)$ reflects the nature of the mixing process. Taylor considered Poiseuille flow in a pipe, where there is no mechanical mixing at all. His result showed $D \propto P_e^2$ in the asymptotic limit, where the characteristic size d is the diameter of the pipe, and the coarse-graining time d^2/D_m is set by the time required by a molecule to sample all the streamlines in the pipe. For porous media a heuristic model of mechanical mixing where streamlines perform a random walk with step length d and a step time of order

$d/\bar{v}$ leads to a dispersion coefficient given by Einstein's result $D = d^2/(d/\bar{v}) \propto P_e$. Saffman modeled a porous medium as a statistically isotropic network of straight capillaries. His calculation leads to $D \propto P_e \log P_e$. Baudet *et al.* [30] show that even for a uniform flow past a sphere, the distribution of residence time is affected by stagnation points and give logarithmic behavior. For a distribution of transit times, for example, Levy distributions [15], one can expect anomalous behavior, i.e., $\sigma^2(t) \propto t^\beta$, $\beta \neq 1$, and a dependence of $D(P_e)$ other than those mentioned above. In simple bead packs we do not expect any such anomalous behavior and, indeed, Ding and Candela [21] find asymptotic behavior in excellent agreement with Saffmann's prediction. It is obvious that in the *preasymptotic* regime, the putative dispersion computed by the ratio σ^2/t need not be a simple function of P_e. NMR and effluent measurements can be expected to produce consistent results for a Gaussian distribution with a well defined dispersion coefficient D, which is predicated upon a mean displacement length much larger than any spatial and permeability correlation lengths, and an experimental time scale long enough to couple all fluid volumes into the mean flow by diffusion. How dispersion depends on L_D can be used as a tool to extract the inhomogeneity length scales associated with stagnation zones. In NMR the range of accessible L_D is set by the NMR relaxation time T_1 and is of order $\sqrt{2D_m T_1}$ or less. Analogous miscible displacement measurements of the skewness as a function of time are the logical complement to the PFG-NMR measurements for longer stagnation length scales.

In conclusion, using the first direct measurement of the third cumulant we quantify the magnitude and sign of deviations of the displacement distribution from a Gaussian shape. We demonstrate that stagnant zones of the flow field in bead packs are smaller than about 0.3 bead diameters, and, most importantly, we demonstrate that data obtained with different fluids and bead sizes can be mapped onto each other when understanding them in terms of a normalized diffusion length and mean displacement. Thus we provide the first conceptually unified experimental picture of preasymptotic dispersion in the canonical physicists' model of a porous medium, the random pack of monodisperse spheres.

We thank E. Dussan, A. Pearson, D. Kroll, and D. Cory for useful discussions and M. Hürlimann, Luca Marinelli, and Lukasz Zielinski for comments on the manuscript.

[1] G. I. Taylor, Proc. R. Soc. London **219**, 186 (1953).
[2] G. I. Taylor, Proc. R. Soc. London **225**, 473 (1954).
[3] P-G. de Gennes, J. Fluid Mech. **136**, 189 (1983).
[4] E. Charlaix, J. P. Hulin, and T. J. Plona, Phys. Fluids **30**, 1690 (1987).
[5] J.-P. Hulin and D. Salin, *Experimental Methods in Physical Sciences* (Academic Press, New York, 1999), Vol. 35.
[6] L. Lebon, L. Oger, J. Leblond, J.-P. Hulin, N. S. Martys, and L. M. Schwartz, Phys. Fluids **8**, 293 (1996).
[7] J. D. Seymour and P. T. Callaghan, J. Magn. Reson., Ser. A **122**, 90 (1996).
[8] J. J. Tessier, K. J. Packer, F-F. Thovert, and P. M. Adler, AIChE J. **43**, 1653 (1997).
[9] B. Manz, P. Alexander, and L. F. Gladden, Phys. Fluids **11**, 259 (1999).
[10] G. A. Barrall, Ph.D. thesis, University of California–Berkeley, 1995.
[11] C. P. Lowe and D. Frenkel, Phys. Rev. Lett. **77**, 4552 (1996).
[12] R. Maier, D. M. Kroll, R. S. Bernard, S. E. Howington, J. F. Peters, and H. T. Davis, Phys. Fluids **12**, 2065 (2000).
[13] P. G. Saffman, J. Fluid Mech. **6**, 321 (1959).
[14] P. G. Saffman, J. Fluid Mech. **6**, 194 (1960).
[15] M. F. Schlesinger, B. J. West, and J. Klafter, Phys. Rev. Lett. **58**, 1100 (1987).
[16] K. H. Coats and B. D. Smith, Soc. Pet. Eng. J. **231**, 73 (1964).
[17] L. E. Baker, Soc. Pet. Eng. J. **263**, 219 (1977).
[18] E. O. Stejskal and J. E. Tanner, J. Chem. Phys. **42**, 288 (1965).
[19] R. M. Cotts, M. J. R. Hoch, T. Sun, and J. T. Markert, J. Magn. Reson. **83**, 252 (1989).
[20] P. T. Callaghan, *Principles of Nuclear Magnetic Resonance Microscopy* (Oxford University Press, New York, 1991).
[21] A. Ding and D. Candela, Phys. Rev. E **54**, 656 (1996).
[22] J. D. Seymour and P. T. Callaghan, AIChE J. **43**, 2096 (1997).
[23] L. Lebon, J. Leblond, and J.-P. Hulin, Phys. Fluids **9**, 481 (1997).
[24] J.-C. Bacri, M. Rosen, and D. Salin, Europhys. Lett. **11**, 127 (1990).
[25] J. Kärger and W. Henk, J. Magn. Reson. **51**, 1 (1983).
[26] M. Toda, R. Kubo, and N. Hashitsume, *Statistical Physics* (Springer-Verlag, New York, 1985), 2nd ed.
[27] Harald Crámer, *Mathematical Methods of Statistics* (Princeton University Press, Princeton, 1999).
[28] H. K. Moffatt, J. Fluid Mech. **18**, 1 (1964).
[29] S. Taneda, J. Phys. Soc. Jpn. **46**, 1935 (1979).
[30] C. Baudet, E. Guyon, and Y. Pomeau, J. Phys. Lett. **46**, L991 (1985).